

Internal oscillations and instability characteristics of $(2+1)$ -dimensional solitons in a saturable nonlinear medium

Jianke Yang*

Department of Mathematics and Statistics, University of Vermont, Burlington, Vermont 05401

(Received 19 April 2002; published 13 August 2002)

Two related problems on scalar $(2+1)$ -dimensional solitons in a saturable nonlinear medium are investigated. The first one is the internal oscillations of fundamental (single-hump) solitons. Internal modes which cause these oscillations, both with and without angular dependence, are discovered. The visual effect of angle-dependent internal modes on the soliton can be a rotation or spatially uneven breathing of the perturbed soliton. These internal oscillations are very robust and persist for a very long distance. The second problem is the instability of double-hump and radially symmetric solitons. Unstable eigenmodes of these solitons are presented. Contrary to intuition, the instability growth rates decrease to zero when the soliton power becomes high. Thus the instability is strongly suppressed at high powers. This phenomenon is corroborated by our direct numerical simulations.

DOI: 10.1103/PhysRevE.66.026601

PACS number(s): 42.65.Tg, 05.45.Yv

I. INTRODUCTION

Spatial solitons are under intensive study these days due to their novel physics as well as application potentials. In $1+1$ dimensions [$(1+1)D$], fundamental (single-hump) solitons for both the Kerr (cubic) and saturable nonlinearities are linearly stable [1,2]. In $2+1$ and $3+1$ dimensions, fundamental solitons with a saturable nonlinearity are stable [3–5], but fundamental Kerr solitons exhibit critical collapse [6,7]. Multihump solitons in a saturable medium are linearly unstable [8,9,4]. Evolution of a Gaussian beam in a $(2+1)D$ saturable medium was studied in [10]. Recurrence of the field as well as azimuthal-symmetry breaking was observed. Internal oscillations of $(3+1)D$ fundamental solitons with saturable nonlinearity were examined in [12]. Radially symmetric internal modes were determined. In addition, it was shown that radiation damping of internal oscillations is very slow (algebraically). Collision of $(3+1)D$ fundamental solitons with saturable nonlinearity was investigated in [11]. Last, there is a large body of work on the stability as well as collision of vector solitons in a saturable nonlinear medium [13–22].

Internal oscillations of stable solitons are important for at least two reasons. The first reason is for the understanding of single-soliton dynamics under perturbations. Laser beams in experiments are rarely perfect soliton states; rather they are solitons perturbed by various experimental factors. In some experiments, regular beam patterns were observed [23]. Such patterns could be induced by internal modes of solitons and be manifestations of internal oscillations. The second and probably more important reason is for the understanding of collision dynamics of such solitons. If internal oscillations exist, solitons during collision can temporarily store some of the translational energy in these internal oscillations and retrieve this energy after the collision. This energy exchange

mechanism can induce very complex collision structures such as window sequences and even fractal structures [24–26]. So far, collisions of $(2+1)D$ and $(3+1)D$ fundamental solitons have been studied to some extent [22,21,11], but a better understanding of such collision processes requires a good knowledge of internal oscillations in these solitons. In $(2+1)D$, robust radially symmetric oscillations of solitons were observed in [10], but it is not clear whether such oscillations are induced by internal modes or radiation modes of the solitons. In addition, the possibility of angle-dependent internal oscillations was not explored. In $(3+1)D$, internal oscillations and radiation damping were investigated in [12]. But again, that study only focused on radially symmetric internal modes. In fact, radially asymmetric internal modes also abound, and they can induce more interesting evolution dynamics to the underlying soliton, as we will see later in this paper.

On the problem of the instability of multihump solitons with saturable nonlinearity in $2+1$ and $3+1$ dimensions, one interesting feature which was implicit but not elaborated upon in [8,9,4] is that the instability growth rate of such solitons is reduced when the soliton power is high (see also [29] for similar results in a cubic-quintic medium). This phenomenon is somewhat unexpected, as conventional wisdom says that higher power leads to stronger instability. Some physicists may argue that this phenomenon is not unexpected since in a saturable medium, changes in the refractive index become smaller as the intensity increases; consequently, the instability is weaker. But this argument does not hold, as for vector solitons with saturable nonlinearity, the instability is stronger when the soliton power is higher [18]. Thus this instability reduction of high-power solitons in [8,4,29] is still an interesting phenomenon. Since experimental techniques on solitons in a saturable nonlinear medium have become quite advanced and many theoretical predictions have been experimentally observed, we believe that this interesting instability suppression behavior of high-power solitons deserves experimental confirmation. To pave its way, more detailed theoretical and numerical investigations are in order.

*FAX: 802-656-2552.

Electronic address: jyang@emba.uvm.edu

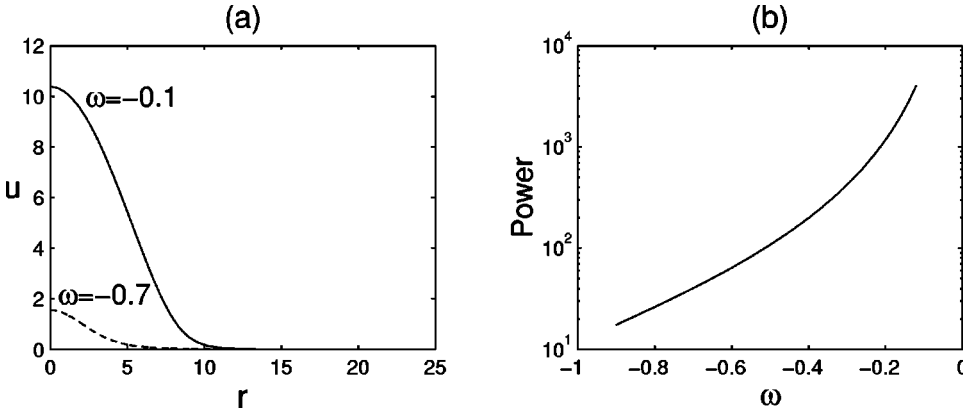


FIG. 1. (a) Fundamental solitons $u(r)$ at $\omega = -0.7$ and $\omega = -0.1$. (b) Power dependence of fundamental solitons on frequency ω .

In this paper, we comprehensively study the stability and instability characteristics of $(2+1)$ -dimensional solitons in a saturable nonlinear medium. For fundamental solitons which are linearly stable in this medium, we determine their internal modes. We will show that both radially symmetric and angle-dependent internal modes exist at high soliton powers. When the soliton power is low, these internal modes disappear. When the soliton power goes to infinity, the frequencies of these modes go to zero. If angle-dependent internal modes are excited, the visual effect can be a rotation or spatially uneven breathing of the perturbed soliton. We also found that these internal oscillations are very robust and radiation damping of these oscillations very weak, similar to the $(3+1)$ D case [12]. As for radially symmetric but double-hump solitons, we will determine all their unstable eigenmodes. Similar to previous findings [8,9], we will show that the instability growth rates of these solitons go to zero in the *high-power* limit as well as the *low-power* limit. Thus, high power serves to *stabilize* double-hump solitons instead of destabilizing it. To confirm this result, we have performed direct numerical simulations of the evolution equation, and good agreement is found between theoretical predictions and numerics. Last, we want to point out that the numerical technique we used for determining internal modes and unstable modes of the above $(2+1)$ D solitons is based on zero-level-contour intersection and successive shooting refinement. This method is more advantageous than that used in [8] which was based on the numerical simulation of the linearized equation. The reason is that, first, our method can conclusively establish the existence or nonexistence of internal modes and unstable modes; second, it is more accurate; third, it applies to the determination of internal modes, where the method of [8] will have some difficulty.

II. INTERNAL MODES OF $(2+1)$ D FUNDAMENTAL SOLITONS IN A SATURABLE MEDIUM

The model for $(2+1)$ -dimensional solitons in an isotropic saturable nonlinear medium is

$$iU_z + \Delta_{\perp} U - \frac{U}{1+|U|^2} = 0, \tag{1}$$

where U is the complex amplitude of the light beam, z is the propagation distance, and Δ_{\perp} is the transverse Laplacian (all quantities are nondimensionalized). We look for radially symmetric solitons of the form

$$U(r, \theta, z) = u(r)e^{i\omega z}, \tag{2}$$

where (r, θ) are the polar coordinates in the transverse plane and ω is the soliton frequency. Then function $u(r)$ satisfies the ordinary differential equation

$$u_{rr} + \frac{1}{r}u_r - \omega u - \frac{u}{1+u^2} = 0, \tag{3}$$

with the vanishing boundary condition $u \rightarrow 0$ as $r \rightarrow \infty$. At $r = 0$, u_r must be zero in view of Eq. (3). When $r \gg 1$ where u is small, Eq. (3) can be linearized. If $\omega > -1$, the linear solution is

$$u(r) = \alpha K_0(\sqrt{1+\omega} r), \tag{4}$$

where $K_0(r)$ is the modified Bessel function and α is a real tail coefficient. Our strategy for finding solitons of Eq. (3) is as follows. For a fixed ω , we vary α in the asymptotic solution (4). At each α , we integrate the nonlinear equation (3) starting from the asymptotic solution (4) at large r toward $r = 0$. If the function $u_r(r=0; \alpha)$ changes sign at certain α values, then these α values give soliton solutions. Carrying out this strategy, we find that for each $-1 < \omega < 0$, there is an infinite, discrete sequence of soliton solutions. The first solution is the fundamental soliton which is strictly positive (the so-called ground state [27]). The second solution crosses zero once, the third solution crosses zero twice, and so on. In this section, we focus on the fundamental soliton which has been known to be stable [4,5]. For illustration, these fundamental solitons at $\omega = -0.7$ and -0.1 are plotted in Fig. 1(a). We see that when ω is larger, the soliton's intensity is higher. If we define the soliton power as

$$P = \int_{-\infty}^{\infty} \int_{-\infty}^{\infty} |U|^2 dx dy = 2\pi \int_0^{\infty} r u^2(r) dr, \tag{5}$$

then the power dependence of fundamental solitons on frequency ω is shown in Fig. 1(b). It is observed that the power

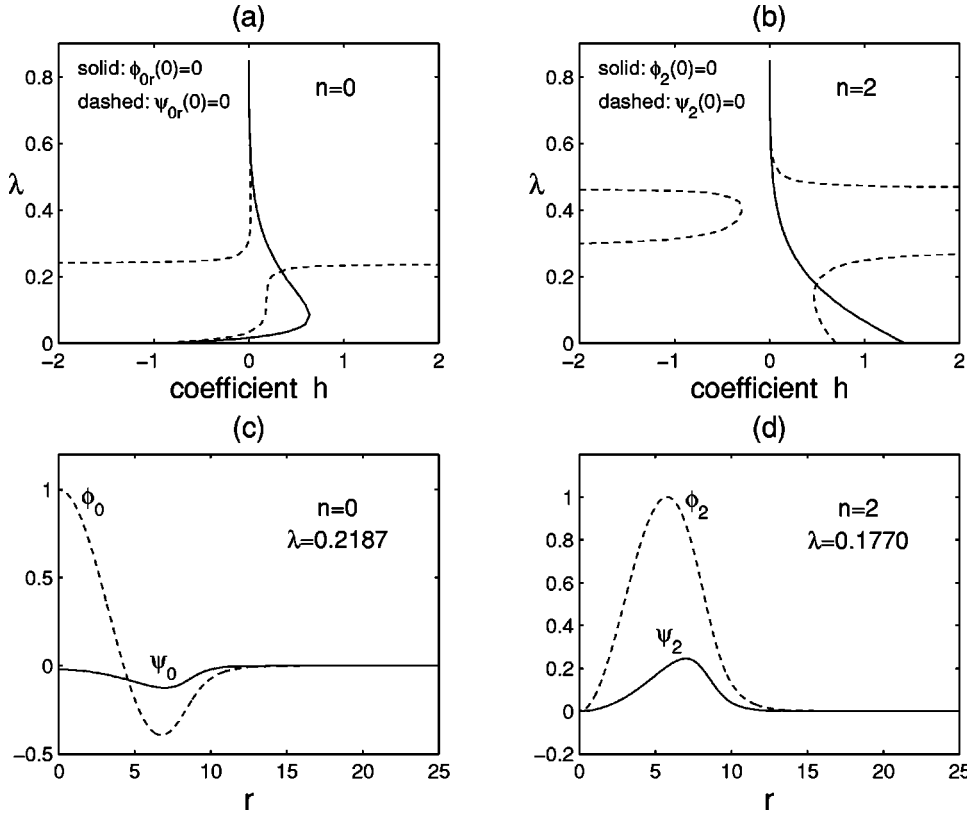


FIG. 2. Our technique for finding internal modes of fundamental solitons. Here $\omega = -0.1$. (a) Zero-level contours of target functions $\phi_{0r}(r=0)$ and $\psi_{0r}(r=0)$ for $n = 0$; (b) zero-level contours of target functions $\phi_{2r}(r=0)$ and $\psi_{2r}(r=0)$ for $n = 2$; (c) the internal mode at $n = 0$; (d) the internal mode at $n = 2$.

is an increasing function of ω . It also appears that the power goes to infinity when ω approaches 0^- . If $\omega > 0$, we have found that $u_r(r=0; \alpha)$ never changes sign for any α value; thus no fundamental solitons exist there. If $\omega < -1$, a continuous family of soliton solutions exists at each ω . However, at large radius r , these solitons are given by Bessel functions; thus they have infinite powers and are unphysical. Hence, in this section, we consider fundamental solitons when $-1 < \omega < 0$.

Since fundamental solitons have been known to be stable, we determine their internal modes next. Internal modes are discrete eigenfunctions of the linearization operator linearized around the soliton. To determine these internal modes, we write the perturbed soliton solution as

$$U(r, \theta, z) = e^{i\omega z} \{ u(r) + \phi_n(r) e^{i(\lambda z + n\theta)} + \psi_n^*(r) e^{-i(\lambda^* z + n\theta)} \}, \quad (6)$$

where $u(r)$ is a fundamental soliton, (ϕ_n, ψ_n) are small perturbations, λ is the eigenvalue, n is an integer representing the angle dependence of the disturbance, and the asterisk (*) represents complex conjugation. When Eq. (6) is substituted into Eq. (1) and higher-order terms in ϕ_n and ψ_n dropped, the eigenvalue problem is

$$\phi_{nrr} + \frac{1}{r} \phi_{nr} - \left(\omega + \lambda + \frac{n^2}{r^2} + \frac{1}{(1+u^2)^2} \right) \phi_n + \frac{u^2}{(1+u^2)^2} \psi_n = 0, \quad (7)$$

$$\psi_{nrr} + \frac{1}{r} \psi_{nr} - \left(\omega - \lambda + \frac{n^2}{r^2} + \frac{1}{(1+u^2)^2} \right) \psi_n + \frac{u^2}{(1+u^2)^2} \phi_n = 0. \quad (8)$$

It is easy to check in Cartesian coordinates that the square of the above linearization operator is self-adjoint; thus the discrete eigenvalue λ is either purely real (internal mode) or purely imaginary (unstable mode). We make two comments here. First, if the soliton (2) is angle dependent (with charge), then the square of its linearization operator is no longer self-adjoint; thus eigenvalues may have both real and imaginary

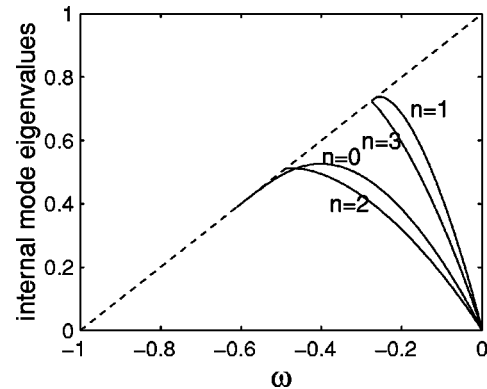


FIG. 3. Internal-mode eigenvalues of fundamental solitons vs frequency ω . Here the dashed line is the edge of the continuous spectrum. Integer n represents the angle (θ) dependence of the internal modes [see Eq. (6)].

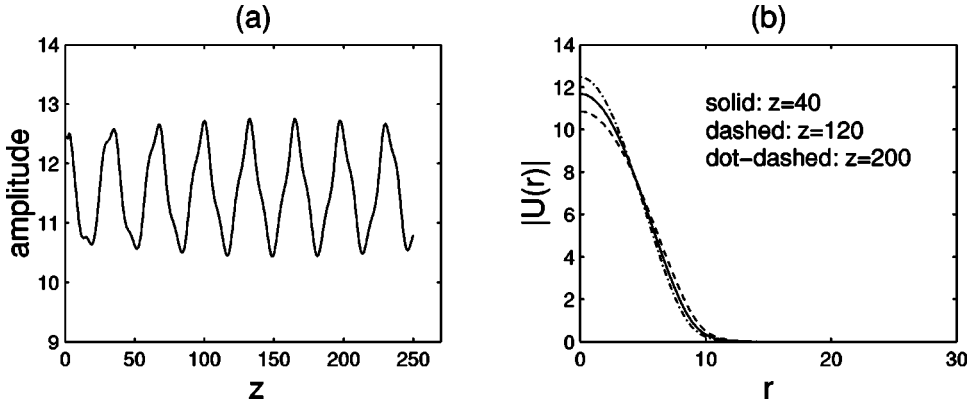


FIG. 4. Evolution of the fundamental soliton with $\omega = -0.1$ under radially symmetric perturbations. The initial perturbed state is given by Eq. (14) where $\epsilon = 0.2$. (a) Distance evolution of the soliton amplitude, i.e., $|U(r=0,z)|$. (b) $U(r,z)$ profiles at three z values.

parts (a similar situation in 1D was discussed in [28]). Second, similar results hold for vector solitons (see [18] for an example).

Next, we exhaustively search for *all* internal modes (purely real eigenvalues λ) of fundamental solitons. In such cases, the eigenfunctions ψ_n and ϕ_n are both real. The boundary conditions for these internal modes are

$$\phi_{0,r}(r=0) = \psi_{0,r}(r=0) = 0, \quad n=0, \quad (9)$$

$$\phi_n(r=0) = \psi_n(r=0) = 0, \quad n \neq 0, \quad (10)$$

and

$$\psi_n \rightarrow 0, \quad \phi_n \rightarrow 0, \quad r \rightarrow \infty. \quad (11)$$

When $-1 < \omega < 0$ and $r \gg 1$, both Eqs. (7) and (8) become a modified Bessel equation whose solutions are

$$\phi_n(r) = K_n(\sqrt{1 + \omega + \lambda} r), \quad (12)$$

$$\psi_n(r) = h K_n(\sqrt{1 + \omega + \lambda} r), \quad (13)$$

where h is a real parameter. Here the coefficient in front of K_n of the eigenfunction ϕ_n has been normalized to be 1 since the eigenvalue problem (7) and (8) is linear. Our strategy for finding all internal modes is the following. At each integer n , we make a large parameter mesh in the two-dimensional h and λ plane. At each (h, λ) mesh point, we numerically integrate Eqs. (7) and (8) starting from a large r value to zero. Due to the boundary conditions (9) and (10), at each n , we check if the target function $\phi_{0,r}(r=0)$ and $\psi_{0,r}(r=0)$ (for $n=0$) or $\phi_n(r=0)$ and $\psi_n(r=0)$ (for $n \neq 0$) zero-level curves in the (h, λ) plane intersect or not. If they do, then the intersection gives an internal mode. If not, then no internal modes at those ω and n values exist. We emphasize that this strategy is rigorous and conclusive, even though it is computer assisted. As two examples, we select $\omega = -0.1$, $n=0$, and $n=2$. The zero contours of respective target functions are shown in Figs. 2(a), 2(b), respectively. As we can see, for $n=0$, the zero-level curves of $\phi_{0,r}(r=0)$ and $\psi_{0,r}(r=0)$ have an intersection at $\lambda \approx 0.2187$ and $h \approx 0.34$. Thus a radially symmetric internal mode with such eigenvalue is discovered. Then, by the shooting method, we can determine this eigenmode to very high accuracy. The eigenfunctions thus obtained are displayed in Fig. 2(c).

These eigenfunctions have been normalized so that the maximum value of ϕ_0 is equal to 1. It is noted that in Fig. 2(a), the zero-level curves of $\phi_{0,r}(r=0)$ and $\psi_{0,r}(r=0)$ also have a trivial intersection at $(\lambda, h) = (0, -1)$. This is the zero eigenvalue which is induced by the phase invariance of the soliton. When $n=2$, we see from Fig. 2(b) that the zero-level curves of $\phi_2(r=0)$ and $\psi_2(r=0)$ have an intersection at $\lambda \approx 0.1770$ and $h \approx 0.49$. Thus an angle-dependent internal mode occurs here. The corresponding eigenfunctions are displayed in Fig. 2(d). Here, the eigenfunctions are also normalized so that the maximum of ϕ_2 is 1. We want to point out that in Figs. 2(a) and 2(b), there is another intersection between these zero-level curves in the upper part of each figure. Since those eigenvalues are close to the edge of the continuous spectrum (which is $\lambda_c = 0.9$ with $\omega = -0.1$), those internal modes are harder to excite from localized perturbations. In this paper, we will not give much attention to those internal modes.

Once we have judiciously discovered internal modes at particular ω and n values by the above algorithm, we then use the shooting method to trace the entire families of internal modes by varying frequency ω . Overall, we have determined the internal-mode families with $n=0, 1, 2$, and 3, and the results are summarized in Fig. 3. Internal modes at higher n values were also discovered, but they are very close to the continuous spectrum and thus will not be considered. Three features of internal modes in Fig. 3 are noted below. The first one is that internal modes with $n=0$ and 2 are the farthest from the continuous spectrum. Thus radiation damping of such modes should be the slowest. In other words, internal oscillations caused by such modes should be most robust. The second feature is that internal-mode eigenvalues go to

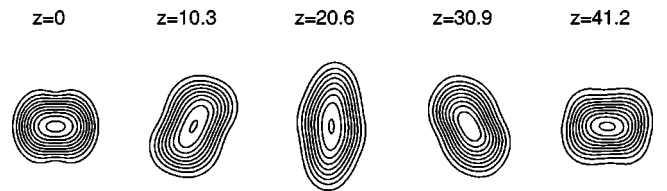


FIG. 5. Evolution of the fundamental soliton with $\omega = -0.1$ under $n=2$ internal-mode perturbations. The initial perturbed state is given by Eq. (15) where $\epsilon = 2$. Here contour levels 1:1:10 of the solution $|U(x,y,t)|$ at five distances are shown. The horizontal direction is x and the vertical direction is y .

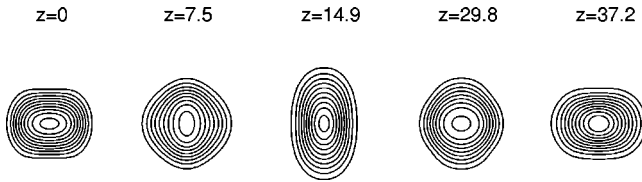


FIG. 6. Evolution of the fundamental soliton with $\omega = -0.1$ under both $n = 2$ and $n = -2$ internal-mode perturbations. The initial perturbed state is given by Eq. (16) where $\epsilon = 2$.

zero when ω approaches 0^- . Recalling that the power of fundamental solitons increases with ω , we see that internal oscillations of high-power solitons are more robust. The third feature is that these internal modes disappear when the soliton power is low.

Next, we numerically study the dynamics of fundamental solitons under the perturbation of these internal modes. We just consider internal oscillations induced by modes $n = 0$ and 2 , as those oscillations are the most persistent (see text above). First, we examine internal oscillations caused by the $n = 0$ mode which is radially symmetric. For simplicity, we take our initial condition as

$$U(r, \theta, z = 0) = (1 + \epsilon)u(r, \omega), \quad (14)$$

where $\epsilon \ll 1$ is a constant perturbation parameter. Obviously, this radially symmetric initial condition will only excite the radially symmetric internal mode of $n = 0$ (and some radiation). Starting from this initial condition, we have simulated the original equation (1). The simulation results with $\epsilon = 0.2$ are displayed in Fig. 4. The left panel of Fig. 4 shows the distance (z) evolution of the soliton amplitude $|U|_{r=0}$. We see that, indeed, a very robust amplitude oscillation is excited. The oscillation frequency is approximately 0.2 , which is close to the $n = 0$ internal-mode frequency (which is 0.2187). To examine radiation damping of these oscillations, we display the radial solution profile $|U(r)|$ at three distances in the right panel of Fig. 4. Remarkably, radiation emission from these internal oscillations is extremely small (almost invisible). Thus, we can expect these oscillations to persist for a very long distance. This finding is consistent with that for $(3 + 1)$ D solitons [12].

Below, we examine internal oscillations caused by the $n = \pm 2$ modes. If the soliton is perturbed only by the $n = 2$ mode, we can write the initial condition as

$$U(r, \theta, z = 0) = u(r, \omega) + \epsilon \{ \phi_2(r) e^{2i\theta} + \psi_2(r) e^{-2i\theta} \} \quad (15)$$

in view of Eq. (6). Simulation of Eq. (1) starting from the above initial condition shows that the internal oscillation induced by the $n = 2$ mode is also very robust. In addition, the effect of this internal-mode perturbation is to prolong the fundamental soliton in one direction, and the evolution visually appears as a *rotation* of the perturbed state. To illustrate, we select $\omega = -0.1$ and $\epsilon = 2$ in the initial condition (15). The fundamental soliton and the internal-mode eigenfunctions can be seen in Fig. 1(a) and Fig. 2(d). Note that since the amplitude of the fundamental soliton at $\omega = -0.1$ is about 10 , thus $\epsilon = 2$ in Eq. (15) is still a small perturbation to the fundamental soliton. With this initial condition, the simulation results at five distances are displayed in Fig. 5. Here the contours of the solution $|U|$ at levels $1:1:10$ are shown at each distance. As we can see, the fundamental soliton under this $n = 2$ internal-mode perturbation appears to rotate counterclockwise. This is an interesting and distinctive visual feature of internal oscillations of solitons in $2 + 1$ dimensions.

If the soliton is perturbed by both the $n = 2$ and $n = -2$ modes, then its evolution is visually different. As an example, we take the $n = \pm 2$ mode components to be equal. Then the initial state of the perturbed soliton can be written as

$$U(r, \theta, z = 0) = u(r, \omega) + \epsilon \{ \phi_2(r) + \psi_2(r) \} \cos 2\theta. \quad (16)$$

With the same parameters $\omega = -0.1$ and $\epsilon = 2$ as above, the contours of the solution at five distances are plotted in Fig. 6. In this case, the perturbed state does not rotate. Instead, it periodically stretches and contracts along orthogonal directions. We can call this behavior as spatially uneven breathing. This uneven breathing is another distinctive visual feature of internal oscillations in $2 + 1$ dimensions. We note that the soliton under $n = 0$ internal-mode perturbations also “breathes,” but that breathing is uniform along all directions.

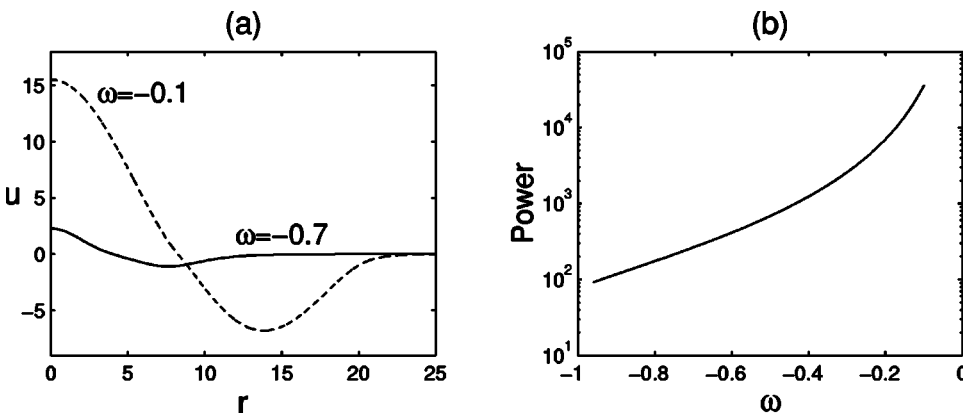


FIG. 7. (a) Double-hump solitons $u(r)$ at $\omega = -0.7$ and $\omega = -0.1$. (b) Power dependence of double-hump solitons on frequency ω .

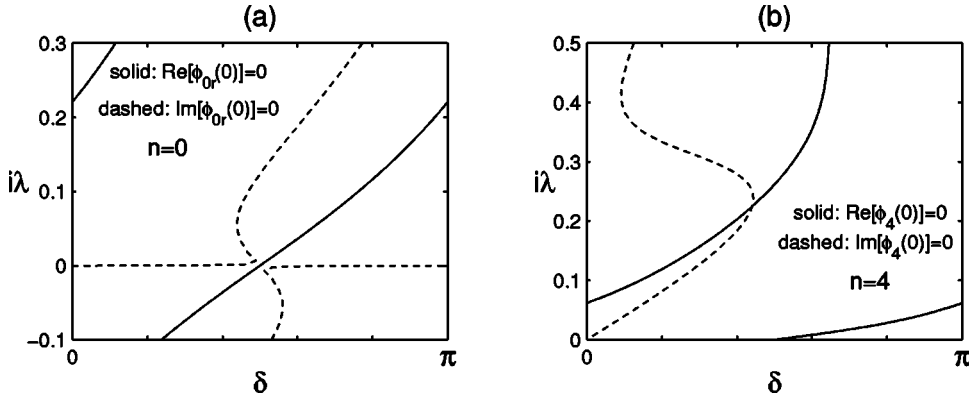


FIG. 8. Our method for finding unstable modes of double-hump solitons. Here $\omega = -0.1$. (a) Zero-level curves of target functions $\text{Re}[\phi_{0r}(r=0)]$ and $\text{Im}[\phi_{0r}(r=0)]$ at $n=0$; (b) zero-level contours of $\text{Re}[\phi_4(r=0)]$ and $\text{Im}[\phi_4(r=0)]$ at $n=4$.

III. INSTABILITY CHARACTERISTICS OF DOUBLE-HUMP SOLITONS

In this section, we study instability characteristics of double-hump solitons whose amplitude functions $u(r)$ cross zero once. The study of solitons with even more humps is similar, and the results are expected to be analogous as well; thus we will not consider such solitons in this paper. It is noted that these double-hump solitons have been shown to be unstable in [8,9]. In this section, we will use a different, more advantageous method to determine the instability growth rates of such solitons. Furthermore, we will use direct numerical simulations of Eq. (1) to corroborate the main features of instability results.

First, we determine the double-hump solitons by the same technique we have used before for fundamental solitons. These double-hump solitons at $\omega = -0.7$ and -0.1 are plotted in Fig. 7(a). The power dependence of these solitons on frequency ω is shown in Fig. 7(b). We see that when ω is larger, the soliton intensity and power are higher, similar to fundamental solitons. Also analogously, physically meaningful double-hump solitons which have finite power exist only when $-1 < \omega < 0$.

Next, we study the linear stability of these double-hump solitons. The perturbed solution is the same as Eq. (6), where $u(r)$ is a double-hump soliton in the present case. The eigenvalue problem is still Eqs. (7) and (8). For double-hump solitons, the square of the linearization operator is still self-adjoint; thus the discrete eigenvalue λ is either purely real (stable) or purely imaginary (unstable). Below, we only search for unstable (purely imaginary) eigenvalues. Our tech-

nique for finding all these unstable eigenvalues is similar to that used in Sec. II, but with some modifications. For a purely imaginary eigenvalue λ , $\psi_n = \phi_n^*$; thus Eqs. (7) and (8) reduce to a single equation (7) for a complex function ϕ_n . The boundary conditions of function ϕ_n are

$$\phi_{0r}(0) = 0, \quad n = 0, \quad (17)$$

$$\phi_n(0) = 0, \quad n \neq 0, \quad (18)$$

$$\phi_n \rightarrow 0, \quad r \rightarrow \infty. \quad (19)$$

When $-1 < \omega < 0$ and $r \gg 1$, Eq. (7) becomes a modified Bessel equation whose solution is

$$\phi_n(r) = e^{i\delta} K_n(\sqrt{1 + \omega + \lambda} r), \quad (20)$$

where δ is a phase constant. Here the eigenfunction ϕ_n has been normalized so that the complex coefficient in front of K_n has magnitude 1. Note that an eigenfunction with phase constant $\bar{\delta} = \delta \pm \pi$ is trivially related to one with phase δ by a multiplication of factor -1 ; thus we can restrict $\delta \in [0, \pi]$ without any loss of generality. Our strategy for finding all unstable eigenvalues is the following. At each integer n , we make a large parameter mesh in the two-dimensional δ and λ plane. At each (δ, λ) mesh point, we numerically integrate Eq. (7) starting from a large r value to zero. If $n = 0$, the eigenfunction must have $\phi_{0r}(r=0; \delta, \lambda) = 0$ [see Eq. (17)]. If $n \neq 0$, it must have $\phi_n(r=0; \delta, \lambda) = 0$ [see Eq. (18)]. Thus at each n , we check if the target function [$\text{Re}(\phi_{0r})$ and $\text{Im}(\phi_{0r})$ or $\text{Re}(\phi_n)$ and $\text{Im}(\phi_n)$] zero-level

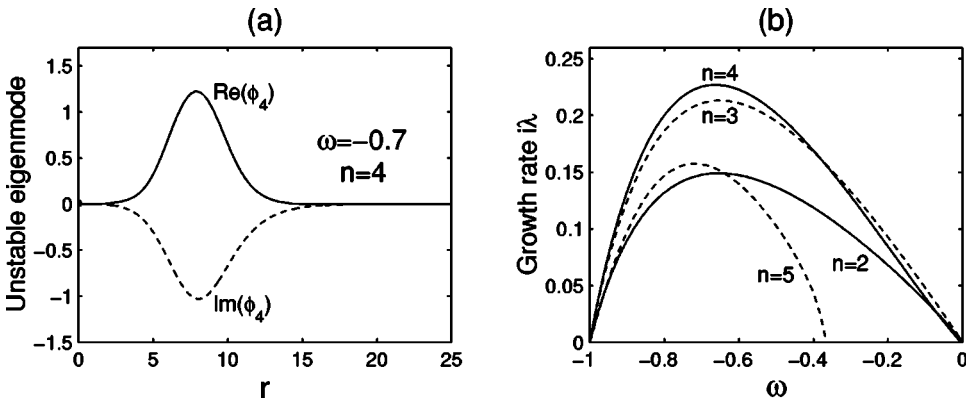


FIG. 9. (a) The unstable eigenmode $\phi_4(r)$ with $n=4$ at $\omega = -0.7$; (b) growth rates of unstable eigenmodes for double-hump solitons vs frequency ω (both solid and dashed lines are unstable eigenvalues).

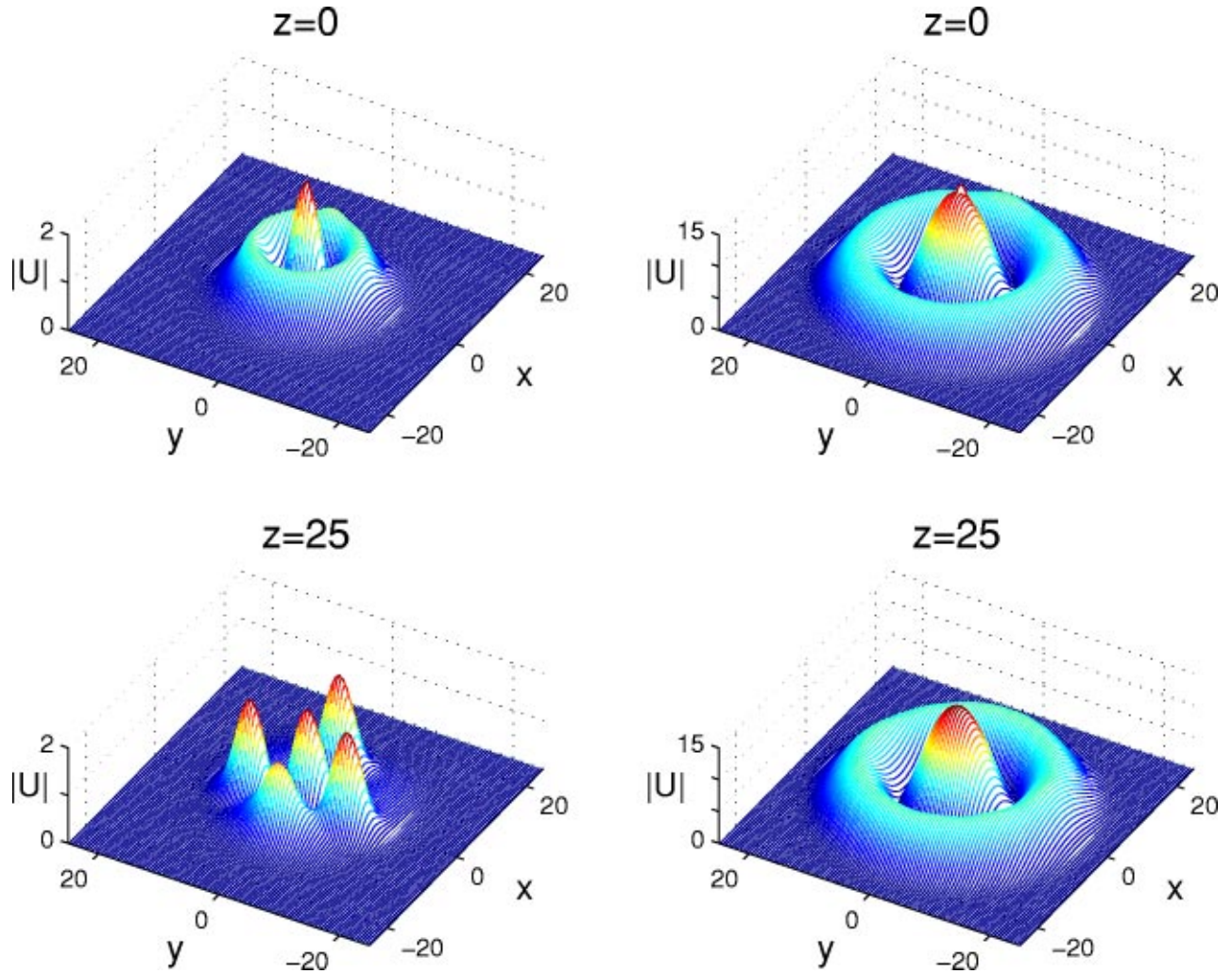


FIG. 10. Strongly suppressed instability of high-power double-hump solitons. Left column: evolution of the perturbed soliton with $\omega = -0.7$ (low power); right column: evolution of the perturbed soliton with $\omega = -0.1$ (high power).

curves in the (δ, λ) plane intersect or not. If they do, then the intersection gives a discrete unstable eigenvalue. If not, unstable eigenvalues at such ω and n values do not exist. To demonstrate, we apply this algorithm to two example cases with $\omega = -0.7$, $n=0$, and $n=4$. The zero-level curves of $\text{Re}(\phi_{0,r})$ and $\text{Im}(\phi_{0,r})$ (for $n=0$) are shown in the left panel of Fig. 8. We see that no intersection occurs here except the trivial one at $(\lambda, \delta) = (0, \frac{1}{2}\pi)$. This intersection corresponds to the zero eigenvalue which is caused by the phase invariance of the soliton. Thus, radially symmetric ($n=0$) unstable modes do not exist. When $n=4$, the zero-level curves of $\text{Re}(\phi_4)$ and $\text{Im}(\phi_4)$ are displayed in the right panel of Fig. 8. Here, however, we clearly see a unique intersection of these zero-level curves at approximately $i\lambda = 0.2253$ and $\delta = 1.43$. Thus, we conclude that there is a single unstable eigenvalue at $\omega = -0.7$ and $n=4$. We then refine this unstable eigenmode by the shooting method, and the eigenfunction is shown in Fig. 9(a).

We have continued this strategy at other ω values and checked those zero-level curves for n from 0 to very large integers. Our findings reveal that for each ω , only up to four

unstable eigenvalues with $n=2, 3, 4$, and 5 could exist. In other words, all unstable eigenmodes have angle dependence in the form $e^{\pm 2i\theta}$, $e^{\pm 3i\theta}$, $e^{\pm 4i\theta}$, or $e^{\pm 5i\theta}$. We have obtained the growth rates ($i\lambda$) of these eigenmodes for all ω values in the interval $(-1, 0)$, and the results are displayed in Fig. 9(b). This figure is almost the same as Fig. 3 in [8] (see also [9]), as it should be, even though our method to obtain this figure is different. As we can see, unstable eigenmodes with $n=2, 3$, and 4 exist for all $-1 < \omega < 0$, while the unstable eigenmode with $n=5$ exists only for $-1 < \omega \lesssim -0.36$. The shapes of these unstable eigenmodes at different n and ω values are quantitatively different but qualitatively similar. They are all equal to zero at $r=0$, have one hump, and decay to zero at $r=\infty$. An example with $\omega = -0.7$ and $n=4$ can be found in Fig. 9(a).

One interesting feature of Fig. 9(b) is that the growth rates of all the unstable eigenmodes decrease to zero not only when $\omega \rightarrow -1$, but also when $\omega \rightarrow 0$. Recalling Fig. 7(b), this means that the instability growth rates diminish not only at low powers, but also at *high* powers. This is a little surprising, as one tends intuitively to expect that solitons with

higher powers are more unstable. But here, it is just the opposite; i.e., high power strongly *suppresses* the soliton instability rather than enhancing it. To verify this suppressed instability, we have simulated Eq. (1) with the initial condition as

$$U(r, \theta, 0) = u(r; \omega) \left(1 + \epsilon + \epsilon \tanh r \sum_{j=1}^{10} \cos j\theta \right), \quad (21)$$

where $u(r; \omega)$ is a double-hump soliton at frequency ω and $\epsilon = 0.01$ is a perturbation parameter. This choice of the initial perturbation was intended to mimic “white noise” perturbations along angle directions. With $\omega = -0.7$ again (low-power soliton), the solutions at $z = 0$ and 25 are shown in the left column of Fig. 10. Here the distance is nondimensionalized by the diffraction length L_D , which in terms of physical units is given by $L_D = \lambda_0 n_0 / (2\pi \Delta n_0)$, where λ_0 is the wavelength of the laser beam, n_0 is the unperturbed refractive index, and Δn_0 is the maximum physical index change. For typical saturable nonlinear materials, $\Delta n_0 / n_0 \approx 2 \times 10^{-4}$. The typical wavelength of lasers used in experiments is approximately $\lambda_0 = 0.5 \mu\text{m}$. For these parameters, the diffraction length is found to be $L_D \approx 0.4 \text{ mm}$. Thus the nondimensional length $z = 25$ in our simulations corresponds to a physical crystal length of about 10 mm. We see from the left column of Fig. 10 that at distance $z = 25$, the double-hump low-power soliton with $\omega = -0.7$ has broken up. Now if we take $\omega = -0.1$ (high-power soliton) and repeat the above simulation, the results are shown in the right column of Fig. 10. Apparently, for the same percentage of initial

perturbations, this high-power double-hump soliton shows little sign of instability at the same distance $z = 25$, which clearly demonstrates the strongly suppressed instability of high-power solitons. Thus, we have verified that, indeed, high-power solitons suffer a drastically reduced instability and are robust.

IV. SUMMARY

In conclusion, we have investigated two major aspects of scalar $(2+1)$ -dimensional solitons in a saturable nonlinear medium. For fundamental solitons, we have found internal modes both with and without angular dependence. Internal oscillations caused by these modes are very robust, especially those caused by modes with no angle dependence ($n = 0$) or with angle dependence in the form $e^{\pm 2i\theta}$ ($n = 2$). Evolution of solitons perturbed by angle-dependent internal modes visually appears like the soliton is rotating or unevenly breathing. For double-hump solitons, we have determined their instability characteristics by a method different from that used in [8]. We have shown that the instability of high-power solitons is very weak, which is unexpected. Thus experimental observation of such solitons is feasible.

ACKNOWLEDGMENTS

The author thanks Yuri Kivshar for bringing Refs. [4,12] to his attention. He also thanks Ziad Musslimani and Boris Malomed for helpful discussions. This work is supported in part by the U.S. Air Force Office of Scientific Research and the National Science Foundation.

-
- [1] V.E. Zakharov and A.B. Shabat, Zh. Éksp. Teor. Fiz. **61**, 118 (1971) [Sov. Phys. JETP **34**, 62 (1972)].
 - [2] G.C. Duree, Jr., J.L. Shultz, G.J. Salamo, M. Segev, A. Yariv, B. Crosignani, P.D. Porto, E.J. Sharp, and R.R. Neurgaonkar, Phys. Rev. Lett. **71**, 533 (1993).
 - [3] M. Mitchell, Z. Chen, M. Shih, and M. Segev, Phys. Rev. Lett. **77**, 490 (1996).
 - [4] D.E. Edmundson, Phys. Rev. E **55**, 7636 (1997).
 - [5] N.G. Vakhitov and A.A. Kolokolov, Izv. Vyssh. Uchebn. Zaved. Radiofiz. **16**, 1020 (1973) [Sov. Radiophys. **16**, 783 (1973)].
 - [6] R.Y. Chiao, E. Garmire, and C.H. Townes, Phys. Rev. Lett. **13**, 479 (1964).
 - [7] L. Berge, Phys. Rep. **303**, 259 (1998).
 - [8] J.M. Soto-Crespo, D.R. Heatley, E.M. Wright, and N.N. Akhmediev, Phys. Rev. A **44**, 636 (1991).
 - [9] N.N. Akhmediev and A. Ankiewicz, *Solitons* (Chapman and Hall, London, 1997).
 - [10] J.M. Soto-Crespo, E.M. Wright, and N.N. Akhmediev, Phys. Rev. A **45**, 3168 (1992).
 - [11] D.E. Edmundson and R.H. Enns, Opt. Lett. **17**, 586 (1992); **18**, 1609 (1993); Phys. Rev. A **51**, 2491 (1995).
 - [12] N.N. Rosanov, S.V. Fedorov, N.A. Kaliteevskii, D.A. Kirsanov, P.I. Krepostnov, and V.O. Popov, Nonlinear Opt. **23**, 21 (2000).
 - [13] M. Mitchell, M. Segev, and D.N. Christodoulides, Phys. Rev. Lett. **80**, 4657 (1998).
 - [14] E.A. Ostrovskaya, Y.S. Kivshar, D.V. Skryabin, and W. Firth, Phys. Rev. Lett. **84**, 1164 (2000).
 - [15] Z.H. Musslimani, M. Segev, D.N. Christodoulides, and M. Soljagic, Phys. Rev. Lett. **84**, 1164 (2000).
 - [16] Z.H. Musslimani, M. Segev, and D.N. Christodoulides, Opt. Lett. **25**, 61 (2000).
 - [17] J.N. Malmberg, A.H. Carlsson, D. Anderson, M. Lisak, E.A. Ostrovskaya, and Y.S. Kivshar, Opt. Lett. **25**, 643 (2000).
 - [18] J.J. Garcia-Ripoll, V.M. Perez-Garcia, E.A. Ostrovskaya, and Y.S. Kivshar, Phys. Rev. Lett. **85**, 82 (2000).
 - [19] T. Carmon, C. Anastassiou, S. Lan, D. Kip, Z.H. Musslimani, and M. Segev, Opt. Lett. **25**, 1113 (2000).
 - [20] W. Krolikowski, E.A. Ostrovskaya, C. Weillnau, M. Geisser, G. McCarthy, Y.S. Kivshar, C. Denz, and B. Luther-Davies, Phys. Rev. Lett. **85**, 1424 (2000).
 - [21] Z.H. Musslimani, M. Soljagic, M. Segev, and D.N. Christodoulides, Phys. Rev. E **63**, 066608 (2001).
 - [22] A.V. Buryak, Y.S. Kivshar, M. Shih, and M. Segev, Phys. Rev. Lett. **82**, 81 (1999).
 - [23] J.W. Grantham, H.M. Gibbs, G. Khitrova, J.F. Valley, and J. Xu, Phys. Rev. Lett. **66**, 1422 (1991).
 - [24] D.K. Campbell, J.F. Schonfeld, and C.A. Wingate, Physica D **9**, 1 (1983).

- [25] P. Anninos, S. Oliveira, and R.A. Matzner, Phys. Rev. D **44**, 1147 (1991).
- [26] J. Yang and Y. Tan, Phys. Rev. Lett. **85**, 3624 (2000).
- [27] M.I. Weinstein, Commun. Pure Appl. Math. **39**, 51 (1986).
- [28] H.T. Tran, J.D. Mitchell, N.N. Akhmediev, and A. Ankiewicz, Opt. Commun. **93**, 227 (1992).
- [29] I. Towers, A.V. Buryak, R.A. Sammut, B.A. Malomed, L.C. Crasovan, and D. Mihalache, Phys. Lett. A **288**, 292 (2001).